CURRENT STATUS OF LUMIO: A LUNAR CUBESAT MISSION AT EARTH-MOON L2

V. Franzese [(1)], G. Merisio [(1)], C. Giordano [(1)], F. Topputo [(1)], A. Cervone [(2)], S. Speretta [(2)], A. Menicucci [(2)], D. Labate [(3)], G. Pilato [(3)], E. Bertels [(4)], A. Thorvaldsen [(5)], J. Vennekens [(6)], R. Walker [(6)]

[(1)] Politecnico di Milano, Via La Masa 34, 20156, Milano, Italy
[(2)] TU Delft, Kluyverweg 1, 2629, Delft, The Netherlands
[(3)] Leonardo, Via delle Officine Galileo 1, 50013, Campi Bisenzio, Florence, Italy
[(4)] ISISpace, Motorenweg 23, 2623 CR Delft, The Netherlands
[(5)] Science and Technology AS, Tordenskiolds Gate 3, 0160, Oslo, Norway
[(6)] ESA/ESTEC, Keplerlaan 1, 2201 AZ, Noordwijk, The Netherlands

ABSTRACT

This work presents the status of the LUMIO mission after completion of the phase A study. The Lunar Meteoroid Impacts Observer (LUMIO) is a 12U CubeSat mission to observe, quantify, and characterise the meteoroid impacts by detecting their flashes on the lunar farside. This investigation complements the knowledge gathered by Earth-based observations of the lunar nearside, thus synthesising a global information on the lunar meteoroid environment. The mission utilises a CubeSat that carries the LUMIO-Cam, an optical instrument capable of detecting light flashes in the visible spectrum. On-board data processing is implemented to minimise data downlink, while still retaining relevant scientific data. The on-board payload data processor autonomously detects flashes in the images, and only those containing events are stored. The mission implements a sophisticated orbit design: LUMIO is placed on a halo orbit about Earth–Moon L_2 where permanent full-disk observation of the lunar farside is made. This prevents having background noise due to Earthshine, and thus permits obtaining high-quality scientific products. Repetitive operations are foreseen, the orbit being in near 2:1 resonance with the Moon orbit. An innovative full-disk optical autonomous navigation experiment is proposed, and its performances are assessed and quantified. These will be validated with respect to the traditional ground-based radiometric tracking. Novel on-board micro-propulsion for orbital control, de-tumbling, and reaction wheels desaturation is used. Steady solar power generation is achieved with solar array drive assembly and eclipse-free orbit. Accurate pointing is performed by using reaction wheels, IMU, star trackers, and fine sun sensors. LUMIO is one of the two winners of ESA's LUCE (Lunar CubeSat for Exploration) SYSNOVA competition, and it is being considered by ESA for near future implementation.

[(1)] V. Franzese, Post-Doctoral Research Fellow, Politecnico di Milano, vittorio.franzese@polimi.it
[(1)] G. Merisio, PhD Candidate, Politecnico di Milano, gianmario.merisio@polimi.it
[(1)] C. Giordano, Post-Doctoral Research Fellow, Politecnico di Milano, carmine.giordano@polimi.it
[(1)] F. Topputo, Full Professor, Politecnico di Milano, francesco.topputo@polimi.it
[(2)] A. Cervone, Assistant Professor, TU Delft, a.cervone@tudelft.nl
[(2)] S. Speretta, Assistant Professor, TU Delft, s.speretta@tudelft.nl
[(2)] A. Menicucci, Assistant Professor, TU Delft, a.menicucci@tudelft.nl
[(3)] D. Labate, Program Manager, Leonardo Company, demetrio.labate@leonardocompany.com
[(3)] G. Pilato, Space CTO/Capability, Leonardo Company, giuseppe.pilato@leonardocompany.com
[(4)] E. Bertels, System Engineer, ISISSpace, e.bertels@isispace.nl
[(5)] A. Thorsvaldsen, Scientific Software Developer, Science and Technology AS Norway, thorvaldsen@stcorp.no
[(6)] J. Vennekens, Satellite Systems Engineer, European Space Agency, johan.vennekens@esa.int
[(6)] R. Walker, Head of CubeSat Systems Unit, European Space Agency, roger.walker@esa.int

1 The LUMIO Mission

<table>
<tr><td colspan="2">LUMIO is a 12U CubeSat mission to a halo orbit at Earth–Moon L2 that shall observe, quantify, and characterize meteoroid impacts on the lunar farside by detecting their impact flashes, complementing Earth-based observations on the lunar nearside, to provide global information on the lunar meteoroid environment and contribute to Lunar Situational Awareness.</td></tr>
<tr><td>Rationale</td><td>An accurate meteoroid flux model in the Lunar environment is fundamental for future humans' outposts on the Moon. Ground-based telescopes cannot observe the Moon far-side, thus scientific information is missing.</td></tr>
<tr><td>Scientific Question</td><td>What are the spatial and temporal characteristics of meteoroids impacting the lunar surface?</td></tr>
<tr><td>Scientific Goal</td><td>To characterize how meteoroids evolve in the cislunar space by observing the flashes produced by their impacts with the lunar surface.</td></tr>
<tr><td>Scientific Objective</td><td>To conduct observations of the lunar surface to detect meteoroids impacts and characterise their flux, magnitudes, energies, and sizes.</td></tr>
<tr><td>Tech-demo Objective</td><td>To demonstrate use of miniaturized technologies, CubeSat operations, and autonomous systems in lunar environment.</td></tr>
<tr><td colspan="2">Phase A Summary</td></tr>
<tr><td>Science</td><td>Payload</td></tr>
<tr><td> 
Scientific objective:
To synthetize a solar system meteoroid flux model by detecting their impact flashes on the Moon farside.</td><td> 
LUMIO-Cam:
○ Visible/Infrared
○ Impacts Detection
○ 6 deg FOV
○ 15 fps
○ Onboard processing</td></tr>
<tr><td>Operative Orbit</td><td>Platform</td></tr>
<tr><td> 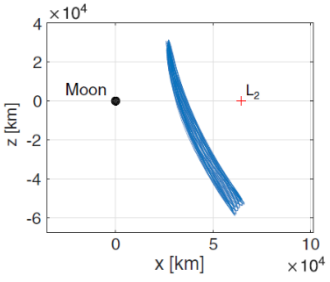
</td><td> 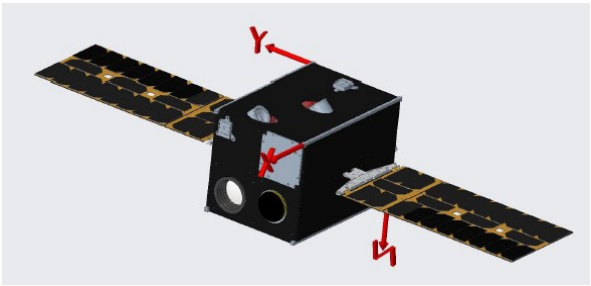 </td></tr>
<tr><td>Halo orbit about Earth-Moon L2 point:
○ ~ 2:1 resonance with E-M period
○ Repetitive operations
○ Permanent lunar far-side observation
○ Eclipse-free
○ Earth always in sight</td><td>Deep-space CubeSat:
○ Size: 12U
○ Mass: ~ 28 kg
○ Power: ~ 60 W
○ Delta-v: ~ 200 m/s
○ Lifetime: 1.5 years</td></tr>
</table>

Table 1: LUMIO Mission Factsheet.

2 INTRODUCTION: SCIENTIFIC MOTIVATIONS

2.1 Relevance

Impacts due to near Earth objects could cause a devastating humanitarian crisis and potentially the extinction of the humans. While the probability of such an event is low, the outcome is so catastrophic that it is imperative to invest resources to mitigate them. Telescopic surveys detect NEOs > 1 km down to 1 meter, but there are few direct methods for monitoring the sub-meter meteoroid population. Meteoroids are small Sun-orbiting fragments of asteroids and comets, whose sizes range from micrometers to meters and masses from 10^{-15} to 10^{4} kg [1]. Their formation is a consequence of asteroids colliding with each other or with other bodies, comets releasing dust particles when close to the Sun, and minor bodies shattering into individual fragments. Meteoroids are hardly detectable even with dedicated surveys. However, they may be observed indirectly when an impact occurs with a planetary or moon solid surface. The ability to accurately predicting these impacts by relying on accurate meteoroid impact flux models is fundamental in many fields.

2.2 Lunar meteoroid impacts

Current estimations of the larger-than-1-kg meteoroid flux at the Moon varies across the literature. The model in [2] estimates 1290 impacts per year, while the one in [3] estimates approximately 4000 impacts per year [4]. More recent studies suggest that the meteoroid impact flux at the Moon is approximately 6 10^{-10} m^2/year, for meteoroids larger than 30 grams [5]. Assuming a lunar collecting area equal to its surface area, 3.8 10^{13} m^2, this gives a larger-than-30-grams meteoroid flux of approximately 23,000 impacts per year. There are also speculations on the possible asymmetries of the spatial distribution of impacts across the lunar surface. In [6], it is theorized that the Moon nearside has approximately 0.1% more impacts than the lunar farside, due to the Earth gravity field; the equatorial flux is 10–20% larger than that at polar regions, due to the higher number of large meteoroids in low orbital inclinations; and the lunar leading side (apex) encounters between 37% to 80% more impactors than the lunar trailing side (antapex), due the Moon synchronous rotation. In a lunar meteoroid impact, the kinetic energy of the impactor is partitioned into 1) the generation of a seismic wave, 2) the excavation of a crater, 3) the ejection of particles, and 4) the emission of radiation. Any of these phenomena can be observed to detect lunar meteoroid impacts. The detection of lunar impact flashes is the most advantageous method since it yields an independent detection of meteoroid impacts, provides the most complete information about the impactor, and allows for the monitoring of a large Moon surface area. Remote observation of light flashes is thus baselined for the detection of lunar meteoroid impacts.

2.3 Sun-Earth-Moon Geometry

The Moon spin–orbit motion is locked into a 1:1 resonance, meaning that an observer on Earth always sees the same portion of the Moon, that is, the lunar nearside. This characteristic, in addition to the fact that a fixed observer on Earth also moves with respect to the Moon, as the Earth rotates about its own axis, constrain the observation of the Moon from the Earth. Since the Moon–Sun synodic period is 29.53 days, the illumination of the lunar nearside varies, which originates the Moon phases. Because lunar impact flashes can only be observed from ground on the lunar nightside and when the lunar nearside is less than 50% illuminated, their detection from Earth is constrained by this Sun–Earth–Moon geometry. Observing the lunar impacts with space-based assets yields several benefits over ground-based telescopes, namely:

- *No atmosphere*. Ground-based observations are biased by the atmosphere that reduces the light flash intensity depending upon present conditions, which change in time. This requires frequent recalibration of the telescope. With the absence of atmosphere in space-based observations, there is no need of recalibrating the instrument and fainter flashes can be detected.
- *No weather*. Ground-based observations require good weather conditions, the lack of which may significantly reduce the observation time within the available window. There is no such constraint in space-based observations.

- *No day/night*. Ground-based observations may only be performed during Earth night, significantly reducing the observation periods. There is no such limitation when space-based observations are performed.
- *Full disk*. Ground-based observations are performed in the first and third quarter, when nearside illumination is 10–50%. Full-disk observations during New Moon are not possible because of low elevation of the Moon and daylight. Space-based observations of the lunar farside can capture the whole lunar full-disk at once, thus increasing the monitored area.
- *All longitudes*. Ground-based observations in the first and third quarter prevent resolving the meteoroid flux across the central meridian. There is no restriction in space-based observations.

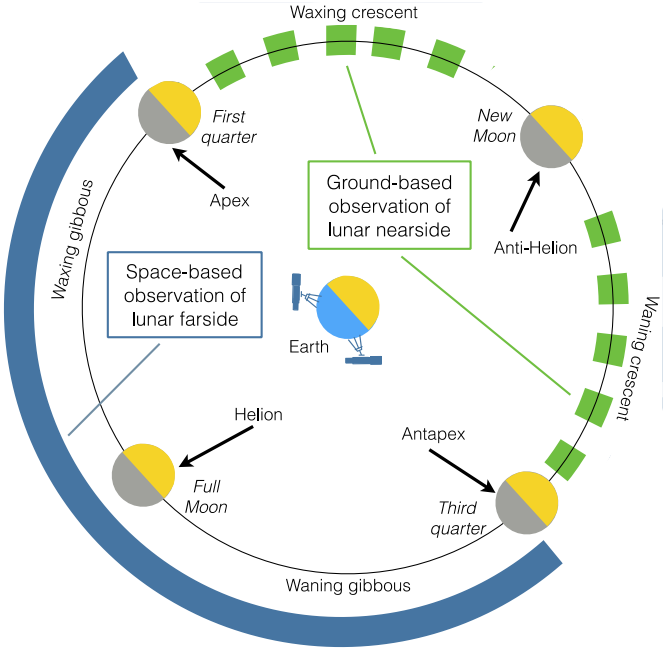

Figure 1: Moon phases and main directions of incoming meteoroids in the Earth-Moon system. The dashed green line represents the portion of the Moon orbit where Earth-based observations of the nearside can be made. The solid blue line indicates the portion of the Moon orbit where space-based observations of the farside can be made.

Moreover, observing the lunar farside with space-based assets yields further benefits, which are the absence of earthshine and the complementarity of observations with respect to the ground-based ones. The absence of Earthshine yields a lower background noise, thus enabling the detection of fainter signals, not resolvable from ground. Then, space-based observations of the lunar farside complement ground-based ones in space and time. In space, the two opposite faces of the Moon are monitored when the Moon is in different orbit locations, while in time, observations are performed in periods when ground-based ones are not possible.

2.4 Lunar Meteoroid Impact Flash Detection

Light flashes at the Moon are observed by detecting a local spike of the luminous energy in the visible spectrum when pointing a telescope at the lunar nightside. The background noise is mainly composed by the Earthshine in the visible spectrum, and by thermal emissions of the Moon surface in the infrared spectrum [7]. Measurements with high signal-to-noise ratios can be obtained through observations of the lunar nightside [8]. The detected luminous energy spike is quantified using the apparent magnitude of the light flash. Lunar impact flashes detected from Earth-based observations have apparent magnitude between +5 and +10.5 [6], which correspond to very faint signals. Also, Earth-based observations of lunar impact flashes are restricted to periods when the lunar nearside illumination is 10–50% [3], [9]. The first unambiguous lunar meteoroid impact flashes were detected during 1999's Leonid meteoroid showers and were reported in [8]. The first redundant detection of sporadic impacts was only reported six years later in [3]. These events gave origin to several monitoring programs. In 2006, a lunar meteoroid impact flashes observation programme was initiated at NASA Marshall Space Flight Center [9]. This facility can monitor 4.5 10^6 km^2 of the lunar surface, approximately 10 nights per month, subject to weather conditions. The most recent monitoring program, NELIOTA, was initiated on February 2017 in Greece under ESA funding. The program aims to detect flashes as faint as +12 apparent visual magnitude [10] and is the first allowing the determination of the impact flash blackbody temperature, by observing both in the visible and infrared spectrum. Monitoring the Moon for impact flashes imposes several restrictions that can be avoided if the same investigation is conducted with space-bases assets.

3 IMPACT FLASH DETECTOR: The LUMIO-Cam

In the LUMIO mission, the observation of the light flashes produced by meteoroid impacts on the Moon far side is performed through the main payload, which is the LUMIO-Cam. The instrument operates between 450 and 950 nm, implementing a double Focal Plane Assembly configuration.

3.1 Payload Requirements

The impact flashes on the Moon can be modelled as black body emissions [6], with temperatures between 2700 K and 6000 K [7], and durations greater than 30 ms [5]. The lowest impact energies correspond to apparent magnitudes higher than 6 as seen from Earth. These characteristics drive the payload requirements, whose high-level ones are listed in Table 2.

Table 2. LUMIO payload high-level requirements.

ID	Requirement
PLD.001	The payload shall detect flashes with energies between 10^{-6} and 10^{-4} kT TNT.
PLD.002	The payload shall detect flashes in the radiation spectrum between 450 nm and 950 nm.
PLD.003	The image integration time shall be equal or greater than 30 ms.
PLD.004	The mass of the payload shall be no more than 4.5 kg.
PLD.005	The maximum power consumption of the payload shall be no more than 20 W.
PLD.006	The maximum size of the payload shall be 10 cm x10 cm x 30 cm.

3.2 Detectors

The LUMIO-Cam uses two detectors, one in the visible band and one in the near infrared band. A dichroic cube has been positioned before the two detectors to split the radiation at 820 nm, enabling the correlation of the impact flashes acquired both in the VIS and NIR band. Having a second measurement in the NIR band will allow reconstructing the temperature of the impact flash based on the ratio between the two observations' magnitude in both VIS and NIR band. Two identical 1024x1024 CCD detectors, namely the CCD201-20 developed by E2V-Teledyne, are positioned after the dichroic cube, shifted by 90 degrees. The detector is a 1024x1024 pixel frame-transfer capable of operating at an equivalent output noise of less than one electron at pixel rates of over 15 MHz. This makes the sensor well-suited for scientific imaging where the illumination is limited and the frame rate is high, as it is for LUMIO. The detector features are reported in Table 3.

Table 3. CCD201-20 detector features.

Parameter	Value	Parameter	Value
Image Area	13.3 mm x 13.3 mm	Low Noise Gain	1 – 1000
Active Pixels	1024 x 1024	Readout Frequency	15 MHz
Pixel Size	13.3 µm x 13.3 µm	Charge Handling Cap.	80ke$^-$/pixel
Storage Area	13.3 mm x 13.3 mm	Readout Noise	< 1 e$^-$ rms

3.3 Optics

Considering the LUMIO orbit (Section 4), for which the S/C-Moon range spans between 35000 and 85000 km, a minimum payload field of view (FOV) of 5.68 deg is necessary to always have the Moon full disk view. To compensate for pointing errors and other effects, a 6 deg FOV is considered for the LUMIO-Cam, leading to a 127 mm focal length (see Table 4).

Table 4. LUMIO-Cam optics features.

FOV	Focal Length	Aperture	F#
6.0 degrees	127 mm	51 mm	2.5

3.4 Mechanical Layout

The mechanical layout of the LUMIO-Cam is shown in Figure 2. It includes a mechanical barrel supporting five lenses, an entrance baffle for out-of-field straylight reduction, two focal plane assemblies, a proximity electronics box, and an external box for mechanical protection. Overall, the instrument dimensions are within 300 mm x 100 mm x 100 mm.

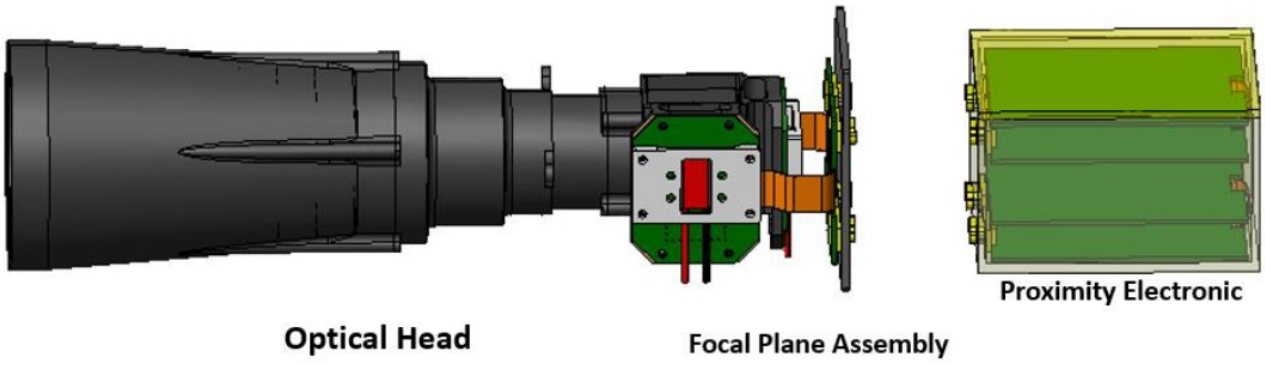

Figure 3. LUMIO-Cam.

3.5 Budgets

The mass and power budgets are reported in Table 5 and Table 6. The LUMIO-Cam total margined mass is 2.88 kg and its worst-case power consumption with margins is 18.84 W.

Table 5. Payload mass budget.

Item	Margin [%]	Margined Mass [kg]
Optics		0.7
Barrel & Baffling		0.7
Electronics		0.8
Harness		0.2
Total		2.4
Total (margined)	20	**2.88**

Table 6. Payload power budget.

Item	Margin [%]	Margined Power [W]
CCDs		7.08
Detectors TEC		4.60
Analog Channels		0.68
FPGA		3.34
Total		15.70
Total (margined)		**18.84**

3.6 Radiometric Analysis

A radiometric analysis employing the LUMIO-Cam properties has been performed to assess the capability of the payload to detect the phenomenon under study. The radiometric analysis has shown that the LUMIO-Cam is capable of detecting an average of 14.000 impacts per year in the energy range 4.9 x 10^{-7} to 5.9 x 10^{-4} kton TNT.

3.7 On-board Payload Data Processing (OBPDP)

On-board image processing is required due to the high amount of data generated by the payload. For an acquisition rate at 15 fps, the data products of the payload would be around 38 TB/day of science acquisitions. Thus, to reduce this amount, the OBPDP detects flashes in the images and stores only 5 frames across the flash delimiting the 50x50 tiles with scientific relevance. In this way, from 559 TB gathered during a LUMIO orbit period (14.7 days), just 144 Mb of data needs to be stored per each scientific orbit, before downloading the science products to ground (Figure 3).

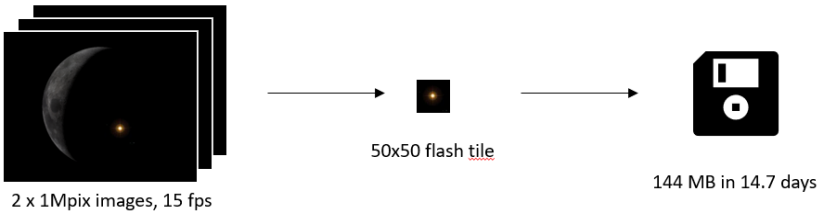

Figure 3: Scientific data amount reduction.

4 MISSION ANALYSIS

The **Earth–Moon L2 halo family is baselined for the LUMIO mission**, after a detailed trade-off of orbit options involving scientific return, safety, coverage, and cost as guiding criteria. It has been shown that remotely detecting flashes on the lunar surface from the halo orbit family is the only technically and economically viable option for a CubeSat [11].

The LUMIO mission is divided in 5 phases, which are (0) the Earth-Moon transfer phase, (1) the Parking Orbit phase, (2) the Transfer phase, (3) the Operative phase, and (4) the End-of-Life phase. In the Earth-Moon transfer phase (0), LUMIO is carried by the deployer till release into a selenocentric parking orbit (1). In this phase, LUMIO performs commissioning and health check before preparing for the stable manifold injection maneuver (SMIM). This maneuver marks the beginning of the transfer phase (2), where two trajectory corrections maneuvers (TCM) and a final halo injection maneuver (HIM) are planned. Then, LUMIO enters in the Operative phase (3), where the operative halo orbit is divided in two cycles: the scientific cycle for continuous processing of images and the engineering cycle for station keeping and platform life checks and corrections. Eventually, after 1 year of operations, LUMIO enters in the End-of-Life phase (4) with a disposal maneuver in a heliocentric orbit. Figure 4 summarizes the LUMIO mission phases.

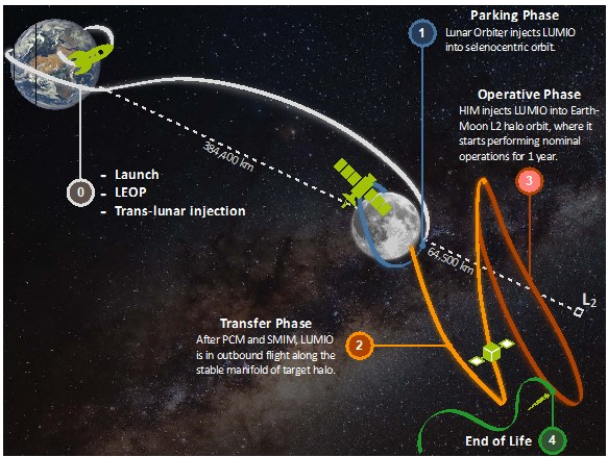

(a) LUMIO Mission Phases

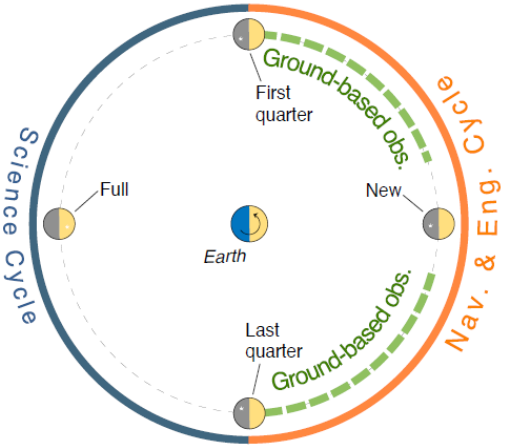

(b) LUMIO Concept of Operations

Figure 4. LUMO mission phases and concept of operations.

4.1 Earth-Moon L_2 quasi-halo orbit

A set of quasi-periodic halo orbits (sometimes referred here as quasi-halos or quasi-halo orbits) about Earth-Moon L_2 are found by employing the methodology described in [12]. Fourteen quasi-halo orbits are computed in the high-fidelity roto-pulsating restricted *n*-body problem (RPRnBP) and saved as SPICE[1] kernels. The initial feeds to compute the quasi-halo samples are Earth-Moon three-body halos at 14 different Jacobi constants, ranging from $C_j = 3.04$ to $C_j = 3.1613263$. The latter value corresponds to the one assumed for the very first iteration of the activities. Although quasi-halos, shown in Figure 5, are computed for a fixed initial epoch, the persistence of libration point orbits in the solar system ephemeris model allows wide freedom in the refinement algorithm, which also includes mission starting at different epochs [13]. Quasi-halo orbits of Figure 5 are all possible LUMIO operative orbits. As the orbit becomes more energetic (or as its CRTBP Jacobi constant decreases), the quasi-halo exhibits a wider range of motion both in terms of a) Moon range and of b) geometrical flight envelope about the corresponding CRTBP trajectory. The latter trend is disadvantageous when a hard-pointing constraint must be respected (e.g., Moon full disk on optical instrument). On the other hand, the lunar distance places a constraint on the minimum FOV for the optical instrument on board LUMIO to resolve the Moon full disk along the quasi-halo.

[1] SPICE is NASA's Observation Geometry and Information System for Space Science Missions [19], [20].

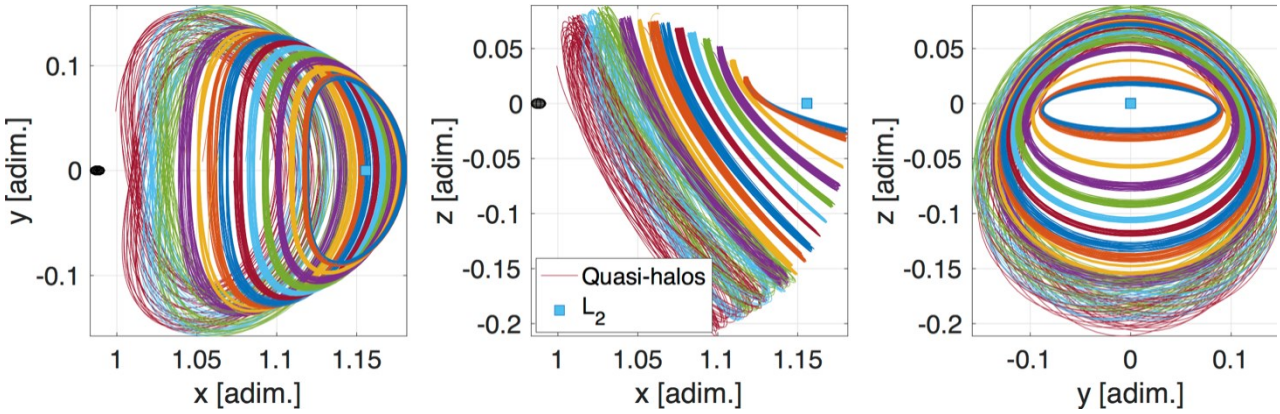

Figure 5. Projection of Earth-Moon L_2 quasi-halos in the roto-pulsating frame.

4.2 Orbital transfer to quasi-halo orbit

The transfer from the selected LLO to the target halo is then propagated in a high-fidelity model. A Multiple Shooting (MS) algorithm is used to refine the transfer trajectory. The instantaneous pericenter and apocenter altitudes are fixed to the one of the selected LLO, while the angular parameters are free to vary. Taking advantage of the holistic search results, the SMIM is performed at its pericenter. The CRTBP stable manifold is used as first guess. The departure date is fixed in February 2024; this date allows the spacecraft to reach the nominal orbit before March 21, 2024, when the scientific phase is expected to start. Tables 7 summarizes the characteristics and the timeline of the high-fidelity transfer from the selected Low-Lunar Orbit to the target halo. Two TCMs are scheduled to occur during the transfer along the stable manifold. TCM1 occurs one day after the Stable Manifold Injection Maneuver, while TCM2 occurs 7 days after the SMIM. The two TCM maneuvers are required to compensate for transfer uncertainties.

Table 7. Low-Lunar Parking Orbit parameters.

Parameter	h_p (km)	h_a (km)	i (deg)	Ω (deg)	ω (deg)	θ (deg)
Value	200	20000	96.4	243.1	260.2	~ 0

4.3 Station-keeping on quasi-halo orbit

Considering the limited Δv capability, fuel consumption for station-keeping around the operative orbits will be a critical factor for mission sustainability. Taking advantage of the generated orbits as reference trajectories, an effort is directed toward the development of a station-keeping strategy that can be used to maintain CubeSats near such nominal LPOs. The S/K cost is estimated by employing the *target points method* (TPM) first introduced in [14], then adapted to the problem of LPOs by [15], and finally used for JAXA's EQUULEUS mission analysis [16]. A massive Monte-Carlo simulation is performed with 10,000 samples, considering the impact of the injection, tracking, and maneuver execution processes on the nominal orbit determined in the presence of solar radiation pressure and gravity of the main solar system celestial bodies (i.e., Sun, 8 planets, the Moon, and Pluto). The errors on orbit injection, orbit determination, and the maneuver execution are all modeled and generated with zero-mean Gaussian distributions, where position, velocity, and maneuver offset covariances are set to 1 km, 1 cm/s, and 2%, respectively. The TPM parameters and the S/K maneuvers epochs are fine-tuned for the LUMIO specific quasi-halos application with a direct simulation technique. Table 8 displays the 1-year S/K cost with its mean value and 3σ confidence, considering a cut-off time of 2 days before the maneuver in the selected operative orbit.

Table 8. Confidence for the 1-year station-keeping cost.

Halo orbit	S/K cost [m/s]		Cut-off Time
Jacobi Constant	Mean (m/s)	3-σ value (m/s)	2 days
3.09	1.86	4.34	

4.4 LUMIO operative orbit

Quasi-halo generated from C_j = 3.09 is the designated LUMIO operative orbit. The selection of LUMIO operative orbit is based on results of the delta-v budget. Indeed, the selected transfer and quasi-halo orbit provides both a) optimality of maneuvers cost, and b) robustness against errors in the actual energy level of the injected stable manifold. Figure 6 shows the LUMIO operative orbit.

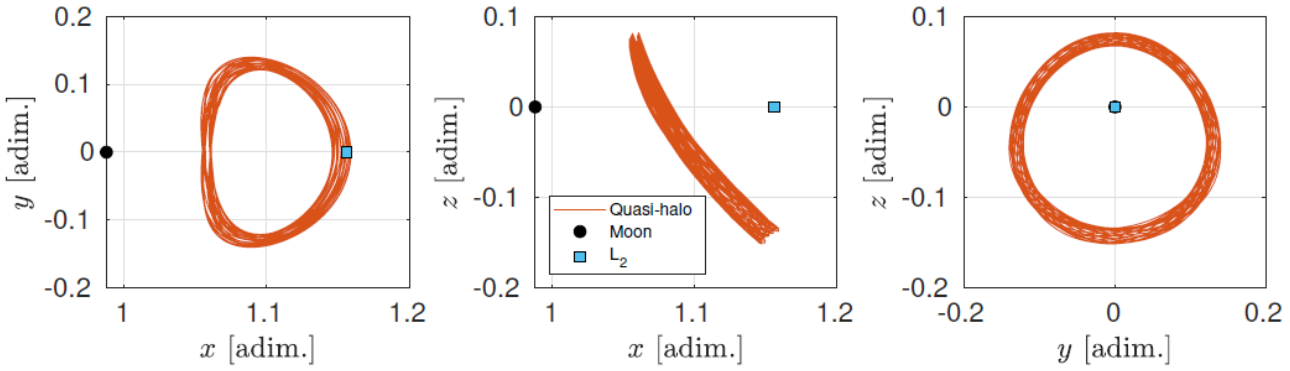

Figure 6: LUMIO Operative Orbit.

4.5 Launch options and budget

The launch opportunities available in the timeframe 2022-2026 are presented. However, the last two options (i.e., Artemis 3 and European Large Logistics Lander (EL3)) have a scheduled launch date too far in the future and, moreover, the possibility of carrying a secondary payload is unclear at the time. For this reason, only the first two options, namely a) CLPS and b) Artemis 2 were considered as possible launch opportunities for LUMIO and selected for deeper analyses.

Table 9: Launch opportunities for LUMIO.

Name	Space Agency	Launch Date	Injection Orbit
CLPS	NASA	From 2022	Low Lunar Orbit
Artemis 2	NASA	2023	Trans-lunar trajectory
Artemis 3	NASA	2024	Low Lunar Orbit
EL3	ESA	2026	Low Lunar Orbit

The mission Δv budgets for each maneuver required to reach the operative orbit and cost for station keeping along the operative orbit considering the CLPS case are reported in Table 10 with both deterministic and confidence values. The total mission delta-v budget for the CLPS launch opportunity case amount to 169.96 m/s (margined). Note that with the Artemis 2 launch opportunity case, the overall delta-v budget for the LUMIO mission amounts to 201.78 m/s.

Table 10. Mission Δv budgets.

Maneuver	Deterministic Cost [m/s]	Stochastic 3-σ [m/s]	Margin [m/s]	Margin [%]
Parking Orbit S/K	0	5.00	5.00	100 %
SMIM	120.00	-	6.00	5 %
TCM1	-	22.00	1.10	5 %
TCM2	-	1.05	0.05	5 %
HIM	4.00	-	0.20	5 %
1-year S/K	-	4.34	0.22	5 %
Disposal	2.00	-	2.00	100 %
TOTAL				169.96 m/s

5 SYSTEM

The LUMIO spacecraft has been designed to perform with a high level of autonomy, particularly for the payload data processing. This choice was driven not only by the operational constraints involved with the observation of the flashes, but also by the ambitious mission design. Additionally, a general zero-redundancy approach has been adopted for all subsystems. This is dictated by the tight mass and volume constraints and a CubeSat design driven risk approach.
In subsystem design, a systematic trade-off procedure has been adopted, based on subsystem specific performance criteria, as well as standard performance, cost and schedule criteria. Consistent design margins have been used for sizing the subsystems based on the development status. A standard 5, 10 and 20% mass margin has been applied for a fully COTS solution, a COTS solution requiring modification and a custom design, respectively.
The most important system and sub-system requirements are summarized in Table 11.

Table 11. Main system and subsystem requirements

ID	Requirement
SYS-01	The mass of the spacecraft shall not be greater than 28 kg.
SYS-02	The spacecraft volume shall not exceed that of a 12U CubeSat.
SYS-03	The satellite shall be able to operate in Lunar environment for at least 1 year.
PROP-01	The propulsion system shall provide a minimum $\Delta V = 204$ m/s for station keeping, orbital transfer, and end-of-life disposal.
PROP-02	The propulsion system shall have a wet mass of no more than 6 kg.
PROP-03	The propulsion system shall have maximum thrusting time of 1 hour per orbital transfer manoeuvre.
PROP-04	The RCS propulsion system shall provide a Total Impulse for all RCS tasks of 110 Ns.
ADCS-01	The spacecraft shall provide an absolute performance error of better than 0.18 deg half-cone during Moon pointing for scientific acquisitions.
ADCS-02	The spacecraft shall provide a relative performance error of better than 5 arcsec over 66.7 ms during Moon pointing for scientific acquisitions.
ADCS-03	The ADCS shall provide a maximum slew rate of 0.5 deg/s.
EPS-01	The EPS shall have a power generation larger than 53.8 W average and a peak power capability of 68 W.
EPS-02	The EPS shall have a mass no more than 3 kg.
COM-01	The spacecraft shall be able to receive commands for more than 95% of all spacecraft orientations in all operational scenarios.
COM-02	The spacecraft telemetry shall be receivable for more than 95% of all spacecraft orientations in all operational scenarios.
COM-03	The communication system shall provide radio navigation support with a position accuracy of 1 km 3-sigma.
PLDP-01	The payload processor shall receive and process at least 15 images per seconds from the payload.
PLDP-02	The payload processors shall identify flashes with SNR greater than 5 dB.
TCS-01	The TCS shall guarantee a temperature range for the payload between -20 deg C and + 50 deg C.
TCS-02	The TCS shall guarantee a temperature range for the internal parts of the system between -10 deg C and + 50 deg C.

5.1 Propulsion

The propulsion system for LUMIO comprehends two systems, one for main propulsion and one for the RCS propulsion. The main propulsion is responsible for the orbital manoeuvring, while the RCS is used for de-tumbling and desaturation of the reaction wheels. An initial trade-off for the main propulsion system has been performed during the LUMIO phase A study. The trade-off criteria were the thrust level, mass, volume, power, schedule/TRL, cost, and compliance with propulsion requirements. It has been found that the mono propellant is the only type of propulsion able to meet all the propulsion requirements for LUMIO. The bi-propellant option requires typical thermal control constraints that would probe to be an issue for the burning times expected by LUMIO. The electric propulsion option has been assessed by the LUMIO mission analysis team and has been ruled out due to the complexity in the orbital transfer and combination of thrust level and power consumption. Cold-gas and electrothermal propulsion are not an option for LUMIO due to their low specific impulse and non-compliance with propulsion requirements. Thus, the current space micro-propulsion market was investigated for available COTS mono-propellant systems, giving special priority to the European market.
Based on the given requirements, two candidates were selected as possible components, which are 1) the NanoAvionics EPSS system and 2) a (partially custom) system developed by Bradford-ECAPS based on their HPGP 1 N thruster. Both solutions are shown in Figure 7. The EPSS mono-propellant system from NanoAvionics is offered with a modular design and several options for scalability. The propellant is ADN-based, with a claimed vacuum specific impulse of 213 s. The system is blowdown, with an initial thrust level of 1 N and a final thrust of 0.22 N, corresponding to a chamber pressure decreasing from 25 bar to 4.7 bar. Bradford, in collaboration with ECAPS, offers a wide range of mono-propellant thruster options in their HPGP (High Performance Green Propulsion) line, characterized also in this case by an ADN-based propellant. Among them, the HPGH 1 N thruster meets the general requirements of LUMIO and has a proven flight heritage, having been qualified in several space missions. This thruster has a vacuum specific impulse in the range from 204 to 231 s, with a proven life of 4272 pulses at a propellant throughput of 1.2 kg. Based on the tailored design solutions offered by both Bradford and NanoAvionics, a final trade-off for the LUMIO main propulsion system was performed. Based on this trade-off, the Bradford-ECAPS HPGP system has been selected as candidate solution for LUMIO and the NanoAvionics system as backup option.

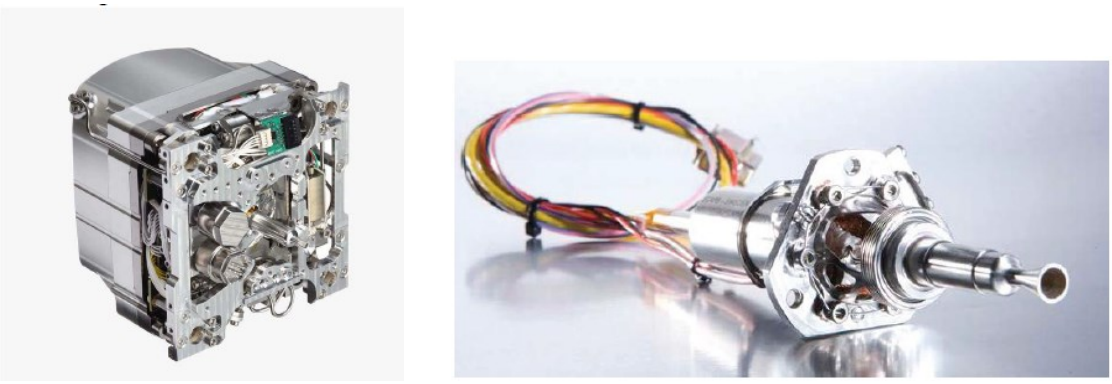

(a) EPSS MonoProp NanoAvionics (b) Bradford-ECAPS

Figure 7: Main propulsion options for LUMIO.

Similarly to what was done for the main propulsion, an initial trade-off was performed for the RCS propulsion to define which type(s) of propulsion would be the most suitable for the task. The trade-off criteria were the thrust level, mass, volume, power, schedule/TRL, cost, and compliance to other requirements. The trade-off has considered the Aurora ARM resistojet and the 6DOF cold gas system produced by GomSpace. As a result of the trade-off, the Aurora ARM resistojet system has been baselined for LUMIO. The characteristics and performance of this system are in line with all requirements. Currently, the GomSpace 6DOF cold gas system does not meet the main requirements (total impulse, mass, volume, power) and would therefore require several adaptions of the spacecraft configuration to become suitable for LUMIO. It is however decided, also in this case, to keep the GomSpace system as backup solution for LUMIO.

5.2 Attitude Determination and Control

The architecture of the ADCS subsystem for LUMIO spacecraft is shown in Figure 8. The sensor suite has been chosen by selecting those with the smallest mass, volume and power budgets complying with the pointing requirements and potential tip-off rates for the whole system.

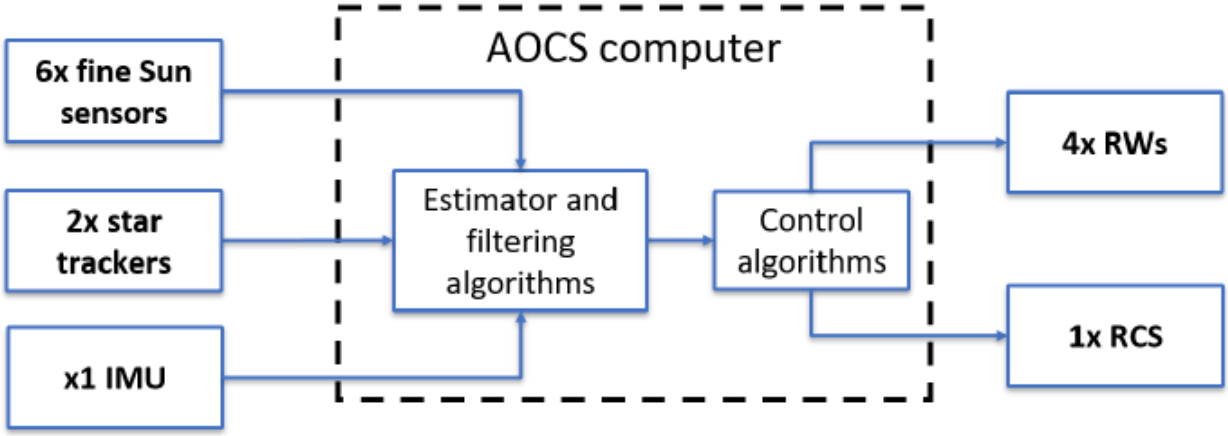

Figure 8: ADCS architecture of the LUMIO spacecraft.

The sensor suite is composed by 6 MAUS Sun sensors produced by Lens R&D (one per CubeSat face), 2 AURIGA star trackers made by Sodern, and 1 Inertial Measurement Unit (IMU) produced by ISISpace. After the trade-off, the sensor suite comprises six MAUS CubeSat Sun sensor, two AURIGA star trackers, and 1 ISISpace IMU. Four reaction wheels in pyramidal configuration have been designed for LUMIO. After the dedicated trade-off, the RW25 SW50 system produced by Astrofein as reaction wheels has been selected. The total impulse budget with the RCS accounts for 160 Ns with a 100% margin. The ADCS routines run on the ISIS onboard computer (iOBC), also used for the navigation algorithm. The complete ADCS system has a mass of 1.63 kg.

5.3 Power

The Electrical Power System (EPS) will consist of a power generation unit in the form of 2 movable solar arrays, a battery pack to store power for moments when a high-power output is required, and a power distribution unit to regulate and distribute the power to the various subsystems. Each solar array presents 24 solar cells. The area of the single cell is equal to 0.003 m2. The cell efficiency is 0.2831. Overall, 48 solar cells are equipped on the two solar arrays, for a total area of 0.144 m2. The peak power consumption is reached in the propulsion heating mode, where 69.35 W are required. The nominal power consumption in science mode is 54.15 W. Given the LUMIO pointing profile and orbit, the power generated by the power system unit is always compatible with the LUMIO power requirements. A Solar Array Drive Assembly (SADA) is designated to correctly point the solar panels to the Sun.

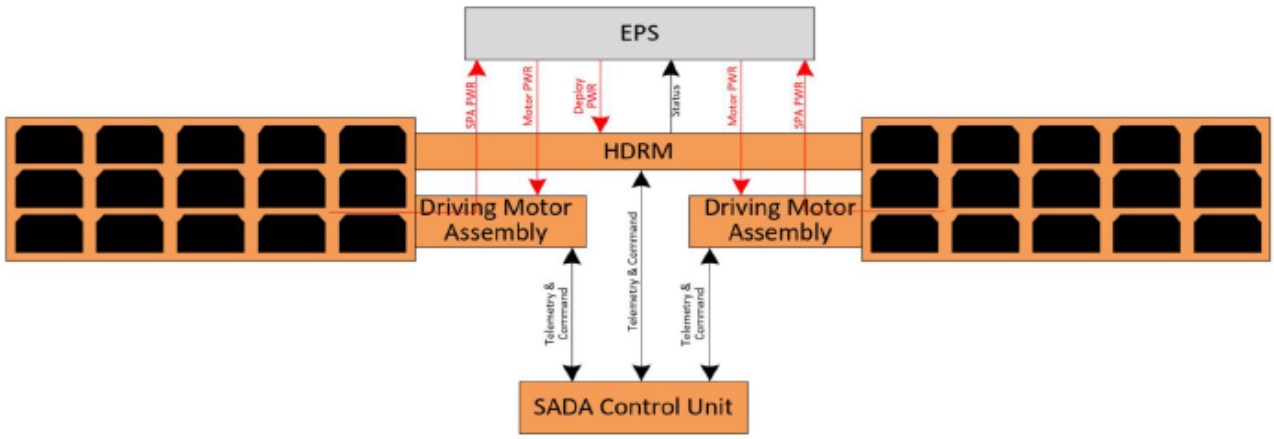

Figure 9: SADA architecture diagram.

5.4 Communication and Navigation

Two architectural solutions have been investigated for communication during the phase A study. These are an Inter-Satellite Link (ISL) using the Lunar Pathfinder spacecraft and a Direct-To-Earth (DTE) link. The ISL is expected to involve, as relay satellite, the SSTL Lunar Pathfinder spacecraft, which is a commercial data relay spacecraft developed by SSTL under ESA contract to service lunar assets. The DTE link is using a traditional configuration with one ground station (in principle, to limit mission cost, but multiple stations can be considered) communicating directly with LUMIO. Thus, both an ISL in S-band and a DTE in X-band links have been selected for LUMIO, where the ISL will be used for commanding the satellite under nominal conditions due to constrained power budget, while the DTE link is used for payload data downlink, ranging, and tracking in nominal conditions. Based on this, the selected radio for the inter-satellite link is the ECW31 produced by Syrlinks with the Anywaves patch antenna in S-band. For the direct-to-Earth link, the radio selected is the IMT C-DST working in the X-band, and two patch antennas have been considered.

An orbit determination analysis has been carried out using Cebreros, ESTRACK ground station and the Sardinia Deep Space ground stations: this analysis has been carried out to verify that the navigation requirements are met. The SDSA (64 meters) located in San Basilio, Cagliari, is assumed as baseline option for the ground communication. The Cebreros, 35 meters antenna, is assumed as backup for the ground communications. In the analysis, these two options are investigated. The assumptions concerning the ground stations are a minimum elevation angle of 15 deg, a range measurements errors (1σ) of 130 m, and a range-rate measurements error (1σ) of 0.2 mm/s. Two-way transparent range measurements have been used at the beginning and end of every ranging session while coherent Doppler measurements have been considered every 20 minutes. An extended Kalman filter estimator was used. During the operative orbit, 40 tracking sessions are expected which results in 120 hours of tracking duration (3 hours each) to which a 20% margin has been added. All in all, the navigation requirements of 1 km and 1 cm/s accuracies are met. LUMIO will also assess the performances of an autonomous navigation method exploiting the Moon apparent size in the images gathered by the LUMIO-Cam [17].

5.5 Structure and Thermal

The main satellite structure is a COTS-based 12U CubeSat structure produced by ISISpace. A detailed radiation analysis has been conducted to define the thickness of the satellite external aluminium panels for sufficient radiation shielding, taking as a reference the LUMIO operational orbit and the position of the Moon for 1 year. SPENVIS's Solar particle model ESP-PSYCHIC (total fluence) was used to calculate the Total Ionizing Dose (TID) and long-term Single Event Upsets for the operational orbit. Then, using SHIELDOSE-2 model, the TID was computed as a function of the thickness of aluminium shielding material of the spacecraft. Since most of the internal spacecraft components can tolerate a TID up to 20 krad and applying a 100% margin on this value due to the large uncertainties in this analysis, a thickness of 1.5 mm was selected, with additional internal shielding foreseen for particularly critical components (IMU, star trackers, SADA). The total mass of the structure designed with this criterion is 4 kg.

The Thermal Control System has been designed to ensure spacecraft thermal stability throughout the mission lifetime, by keeping all subsystems within their acceptable temperature ranges. Currently, the satellite is modeled as a 12U structure, with each panel representing a node. In addition, all stacks have been modeled as the structure ribs and frames. Input power is applied directly to these ribs, simulating the heat load of a particular stack. As no eclipses were found during the entire duration of the mission, the cold case is found at the operational orbit where the least amount of power is flowing through the system. The hot case happens when the spacecraft is illuminated with the maximum exposed surface and the spacecraft is in its science mode. Results showed that, with a combination of three different thermal coatings (27% gold, 25% silvered Teflon, 48% polished Al 6061-T6), the spacecraft temperature stays in a range from -5 to +45 ºC when illuminated by the Sun, which is compliant with the thermal requirements of LUMIO.

5.6 Command and Data Handling and Onboard Payload Data Processor

The current LUMIO spacecraft design is based on three separate On-Board computer units: one for the ADCS sub-system and one for the main OBC, for both of which the iOBC computer produced by ISISpace will be used, and then, an on-board payload data processing unit itself.

5.7 Spacecraft Configuration and budget

Figure 10 shows the current foreseen configuration for the LUMIO spacecraft, while the complete mass and power budgets, including margins at system and subsystem level, are shown in Table 12. A total margined mass of 28.66 kg is currently estimated for the spacecraft. This is expected to be reduced in further phases to comply with the requirement of 28 kg maximum mass.

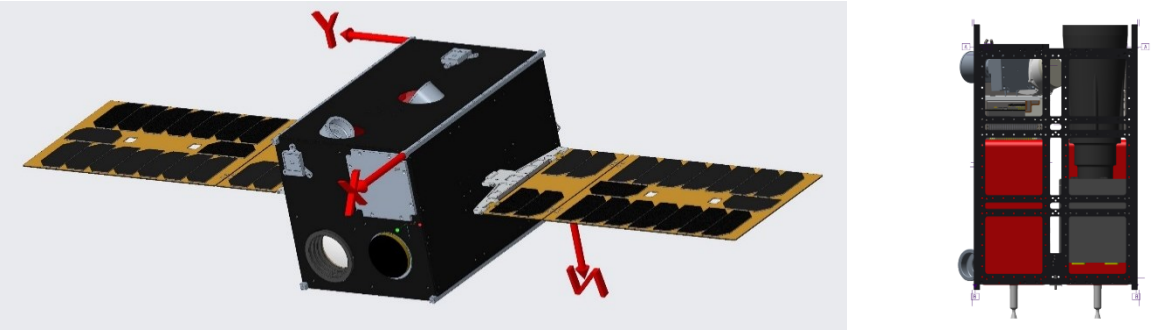

Figure 10. LUMIO spacecraft in deployed configuration (left) and internal view (right).

Table 12. Mass budget of the LUMIO spacecraft, including system and subsystem margins.

Acronym	Subsystem	Mass [kg]
P/L	Payload	3.09
PDT	Payload Data Transfer System	5.06
EPS	Electric Power System	2.83
CDHS	Command & Data Handling System	0.11
TTC	Telemetry, Tracking, and Control	0.32
AOCS	Attitude and Orbit Control	1.63
PROP	Propulsion	4.00
STRUC	Structure	3.70
MISC	Harness	0.33
DRY MASS	Total Dry Mass	21.09
MARGIN	20 % system margin	4.88
PROPELLANT	Propellant	3.29
MARGIN	2 % propellant margin	0.07
TOTAL WET MASS		**28.66**

Table 12: Power consumption per operational mode.

Acronym	Mode	Power [W]
SCI	Science	54.15
PROP	Propulsion Heating	69.35
TRANSFER	Transfer	56.16
RANGING	Ranging	34.08
P/L TX	Payload Tx mode	47.74
RW DESAT	Reaction wheels desaturation	43.24
NOMINAL	Nominal	7.87
SAFE	Safe	37.17
SLEEPING	Sleeping	0.00

6 CONCLUSIONS

The primary science goal of LUMIO mission is to observe meteoroid impacts on the lunar farside to study the characteristics of meteoroids and to improve the meteoroid models. This will improve the understanding of the meteoroid fluxes in the Solar System, which is crucial for future human outposts on the Moon. The LUMIO mission complements ground-based observations with remote space-based observations, so improving the lunar situational awareness. The mission utilizes a 12U form-factor CubeSat which carries the LUMIO-Cam, an optical instrument capable of detecting light flashes in the visible spectrum to continuously monitor and process the data. The mission implements a novel orbit design and latest CubeSat technologies to serve as a pioneer in demonstrating how CubeSats can become a viable tool for deep space science and exploration.

LUMIO has been awarded winner (ex aequo) of ESA's LUCE (Lunar CubeSat for Exploration) SYSNOVA competition and then, LUMIO has successfully completed its phase A study. As such, it is being considered by ESA for implementation soon.

7 REFERENCES

[1] Z. Ceplecha *et al.*, "*Meteor Phenomena and Bodies,*" Sp. Sci. Rev., vol. 84, no. 3, pp. 327–471, 1998.

[2] P. Brown, R. E. Spalding, D. O. ReVelle, E. Tagliaferri, and S. P. Worden, "*The flux of small near-Earth objects colliding with the Earth.,*" Nature, vol. 420, no. 6913, pp. 294–296, 2002.

[3] J. L. Ortiz *et al.*, "*Detection of sporadic impact flashes on the Moon: Implications for the luminous efficiency of hypervelocity impacts and derived terrestrial impact rates,*" Icarus, 184, pp. 319–326, 2006.

[4] T. V Gudkova, P. H. Lognonné, and J. Gagnepain-Beyneix, "*Large impacts detected by the Apollo seismometers: Impactor mass and source cutoff frequency estimations,*" Icarus, vol. 211, no. 2, pp. 1049–1065, 2011.

[5] R. M. Suggs, D. E. Moser, W. J. Cooke, and R. J. Suggs, "*The flux of kilogram-sized meteoroids from lunar impact monitoring,*" Icarus, vol. 238, Supplement C, pp. 23–36, 2014.

[6] J. Oberst *et al.*, "*The present-day flux of large meteoroids on the lunar surface--A synthesis of models and observational techniques,*" Planet. Space Sci., vol. 74, pp. 179–193, 2012.

[7] S. Bouley *et al.*, "*Power and duration of impact flashes on the Moon: Implication for the cause of radiation,*" Icarus, vol. 218, no. 1, pp. 115–124, 2012.

[8] L. R. Bellot Rubio, J. L. Ortiz, and P. V Sada, "*Luminous Efficiency in Hypervelocity Impacts from the 1999 Lunar Leonids,*" Astrophys. J. Lett., vol. 542, pp. L65--L68, 2000.

[9] R. M. Suggs, W. J. Cooke, R. J. Suggs, W. R. Swift, and N. Hollon, "*The NASA Lunar Impact Monitoring Program,*" Earth. Moon. Planets, vol. 102, no. 1, pp. 293–298, 2008.

[10] A. Z. Bonanos *et al.*, "*NELIOTA: ESA's new NEO lunar impact monitoring project with the 1.2m telescope at the National Observatory of Athens,*" in *Proceedings of the International Astronomical Union*, 2015, vol. 10, no. S318, pp. 327–329.

[11] F. Topputo *et al.*, "*Lunar Meteoroid Impacts Observer.*" 2016.

[12] D. A. D. Tos and F. Topputo, "*On the advantages of exploiting the hierarchical structure of astrodynamical models,*" Acta Astronaut., vol. 136, pp. 236–247, 2017.

[13] D. A. Dei Tos and F. Topputo, "*Trajectory refinement of three-body orbits in the real solar system model,*" Adv. Sp. Res., vol. 59, no. 8, pp. 2117–2132, 2017.

[14] N. P. Dwivedi, "*Deterministic optimal maneuver strategy for multi-target missions,*" J. Optim. Theory Appl., vol. 17, no. 1, pp. 133–153, 1975.

[15] K. C. Howell and H. J. Pernicka, "*Stationkeeping method for libration point trajectories,*" J. Guid. Control Dyn., vol. 16, p. 151, 1993.

[16] K. Oguri *et al.*, "*EQUULEUS mission analysys: design of the science orbit phase,*" in *26th International Symposium on Space Flight Dynamics*, 2017, no. 72, pp. 1–7.

[17] V. Franzese, P. Di Lizia, and F. Topputo, "*Autonomous Optical Navigation for the Lunar Meteoroid Impacts Observer*", Journal of Guidance, Control, and Dynamics, 2019, DOI: 10.2514/1.G003999

[18] SRE-PA & D-TEC staff, "*Margin philosophy for science assessment studies,*" 2012.

[19] C. H. Acton Jr, "*Ancillary data services of NASA's navigation and ancillary information facility,*" Planet. Space Sci., vol. 44, no. 1, pp. 65–70, 1996.

[20] C. H. Acton Jr, N. Bachman, B. Semenov, and E. Wright, "*A look towards the future in the handling of space science mission geometry,*" Planet. Space Sci., vol. 150, pp. 9–12, 2018.